

NASA/TP-2005-213931



MOEMS Modeling Using the Geometrical Matrix Toolbox

William C. Wilson
Langley Research Center, Hampton, Virginia

Gary M. Atkinson
Virginia Commonwealth University, Richmond, Virginia

October 2005

The NASA STI Program Office . . . in Profile

Since its founding, NASA has been dedicated to the advancement of aeronautics and space science. The NASA Scientific and Technical Information (STI) Program Office plays a key part in helping NASA maintain this important role.

The NASA STI Program Office is operated by Langley Research Center, the lead center for NASA's scientific and technical information. The NASA STI Program Office provides access to the NASA STI Database, the largest collection of aeronautical and space science STI in the world. The Program Office is also NASA's institutional mechanism for disseminating the results of its research and development activities. These results are published by NASA in the NASA STI Report Series, which includes the following report types:

- **TECHNICAL PUBLICATION.** Reports of completed research or a major significant phase of research that present the results of NASA programs and include extensive data or theoretical analysis. Includes compilations of significant scientific and technical data and information deemed to be of continuing reference value. NASA counterpart of peer-reviewed formal professional papers, but having less stringent limitations on manuscript length and extent of graphic presentations.
- **TECHNICAL MEMORANDUM.** Scientific and technical findings that are preliminary or of specialized interest, e.g., quick release reports, working papers, and bibliographies that contain minimal annotation. Does not contain extensive analysis.
- **CONTRACTOR REPORT.** Scientific and technical findings by NASA-sponsored contractors and grantees.

- **CONFERENCE PUBLICATION.** Collected papers from scientific and technical conferences, symposia, seminars, or other meetings sponsored or co-sponsored by NASA.
- **SPECIAL PUBLICATION.** Scientific, technical, or historical information from NASA programs, projects, and missions, often concerned with subjects having substantial public interest.
- **TECHNICAL TRANSLATION.** English-language translations of foreign scientific and technical material pertinent to NASA's mission.

Specialized services that complement the STI Program Office's diverse offerings include creating custom thesauri, building customized databases, organizing and publishing research results ... even providing videos.

For more information about the NASA STI Program Office, see the following:

- Access the NASA STI Program Home Page at <http://www.sti.nasa.gov>
- E-mail your question via the Internet to help@sti.nasa.gov
- Fax your question to the NASA STI Help Desk at (301) 621-0134
- Phone the NASA STI Help Desk at (301) 621-0390
- Write to:
NASA STI Help Desk
NASA Center for AeroSpace Information
7121 Standard Drive
Hanover, MD 21076-1320

NASA/TP-2005-213931



MOEMS Modeling Using the Geometrical Matrix Toolbox

William C. Wilson
Langley Research Center, Hampton, Virginia

Gary M. Atkinson
Virginia Commonwealth University, Richmond, Virginia

National Aeronautics and
Space Administration

Langley Research Center
Hampton, Virginia 23681-2199

October 2005

The use of trademarks or names of manufacturers in the report is for accurate reporting and does not constitute an official endorsement, either expressed or implied, of such products or manufacturers by the National Aeronautics and Space Administration.

Available from:

NASA Center for AeroSpace Information (CASI)
7121 Standard Drive
Hanover, MD 21076-1320
(301) 621-0390

National Technical Information Service (NTIS)
5285 Port Royal Road
Springfield, VA 22161-2171
(703) 605-6000

Available electronically at <http://ntrs.nasa.gov/>

Abstract

New technologies such as MicroOptoElectro-Mechanical Systems (MOEMS) require new modeling tools. These tools must simultaneously model the optical, electrical, and mechanical domains and the interactions between these domains. To facilitate rapid prototyping of these new technologies an optical toolbox has been developed for modeling MOEMS devices. The toolbox models are constructed using MATLAB's[®] dynamical simulator, Simulink[®]. Modeling toolboxes will allow users to focus their efforts on system design and analysis as opposed to developing component models. This toolbox was developed to facilitate rapid modeling and design of a MOEMS based laser ultrasonic receiver system.

I. Introduction

This document uses a Micro OptoElectroMechanical Systems (MOEMS) based laser ultrasonic receiver system as a working example to describe the modeling and simulation capabilities of the MOEMS toolbox. The system level model employs a top down design approach that hierarchically breaks down the laser ultrasonic receiver into manageable components. The toolbox models micro optical components commonly referred to as MOEMS devices. These component models take into account micro optical phenomena such as losses due to etch holes. Each component is modeled using matrix geometrical optic methods and image processing. The optical models employ geometrical system matrices for calculations involving both the focus and magnification factor. The inputs and outputs of each component consist of an image for dynamical manipulation and a state vector. The system model includes a test bench that simulates input stimuli and models the behavior of the material under test conditions. The components modeled include: thick lenses, mirrors, beam splitters, wave plates, and an optical detector. The wave plates are modeled using rotational matrices, while the other optical components incorporate the paraxial matrix methods. Other effects taken into account in the system model are the optical losses incurred due to etch-hole size and spacing.

The primary purpose of the system model is not only to determine the feasibility of design but

also to identify which component parameters are critical for achieving the design specifications. In addition, the MOEMS toolbox can also be used for rapid prototyping of optical systems. Example problems that can be quickly solved include those with compound lenses and multiple component systems. Key ideas to stress when using this toolbox are Geometrical Matrix Optical methods, top down, and hierarchical design methodologies and system design of MOEMS systems.

II. Modeling Approach

The first step in top-down design methodology used in this example is to separate the laser ultrasonic MOEMS receiver system into a hierarchy of sub-components. The individual components are then modeled using a hybrid approach involving both geometrical matrix optical modeling and image processing. The calculations are performed by MATLAB'S[®] dynamical simulator, Simulink[®]. Both an optical image and a state vector are passed to each component. The state vector is comprised of the following information: paraxial angle, paraxial height, phase angle, direction angle x, direction angle y, direction angle z, distance from preceding element, height of beam plane, and width of beam plane. Geometrical matrices are calculated for each component and used to modify the image dynamically. This information is used to calculate the modifications to the image and the new state vector that is passed on to the next component.

Simulink[®] is a dynamical simulator and as such can perform image processing using plane waves in conjunction with the geometrical matrix modeling. Matlab's[®] Image toolbox can be used for manipulating an image, under the control of the MOEMS toolbox. Functions such as resizing of images, image intensity scaling, and others can be modified under the direction of the optical components discussed.

The image processing for our initial application is based upon planar wave fronts, where each image represents the current phase of the wave front at that instance in time. The phase of the wave front is modeled using a sinusoidal source that modulates the intensity. This would allow for superposition of the waves to generate images such as fringe patterns. To date we have only used a single pixel of the image to generate the output signal. The detector we have modeled is not an array; therefore a single pixel is an accurate representation of the output from a Photo-EMF type of sensor. In the future we hope to create system models using the components of the toolbox that will perform more elaborate image processing.

III. Modeling Technique

A. Geometrical Matrices

Geometrical matrix optical modeling techniques are based upon the paraxial assumptions, which state that the angles involved with ray tracing must be close to zero. In other words, the angles must be very close to parallel to the optical axis. Trigonometric functions can then be simplified, since $\sin(\theta) \sim \theta$, and $\cos(\theta) \sim 1$, for very small values of θ . This approximation allows the tracing of rays to be accomplished using simple matrix manipulations. For example (See Fig. 1), if a ray translates a distance t_1 , through a medium with index of refraction n_1 , starting with height h , and the ray has an initial angle θ , then the new height h_1 , and new angle θ_1 , can be calculated using the following matrix equation.

$$\begin{pmatrix} \theta_1 \\ h_1 \end{pmatrix} = \begin{pmatrix} 1 & 0 \\ \frac{t_1}{n_1} & 1 \end{pmatrix} \cdot \begin{pmatrix} \theta \\ h \end{pmatrix} \quad (1)$$

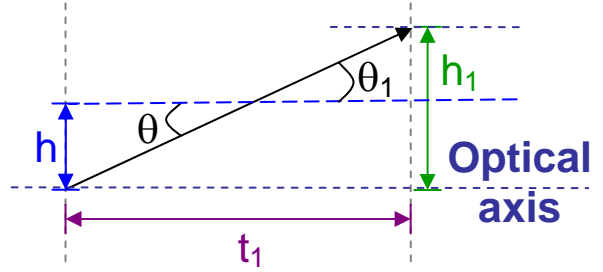


Fig. 1. Geometry of a ray translation.

Similarly, the case of refraction of a light wave can be handled using matrices (See Fig. 2). In this case, if a ray translates through a medium with index of refraction n_1 , starting with height h , and initial angle θ , then the ray encounters a material with index of refraction n_2 and radius of curvature r_1 , the new height h_1 , and new angle θ_1 , can be calculated using the following matrix equation.

$$\begin{pmatrix} \theta_1 \\ h_1 \end{pmatrix} = \begin{pmatrix} 1 & \frac{-(n_2 - n_1)}{r_1} \\ 0 & 1 \end{pmatrix} \cdot \begin{pmatrix} \theta \\ h \end{pmatrix} \quad (2)$$

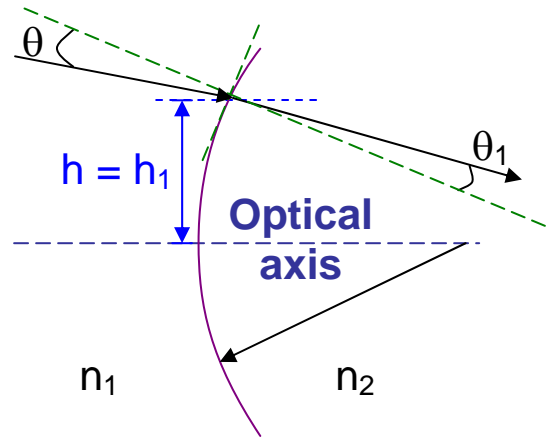


Fig. 2. Geometry of a ray experiencing refraction.

The final case to investigate is when a ray is reflected from a surface of a material (See Fig. 3). In this case, if a ray is traveling through a medium with index of refraction n_1 , starting with height h , and initial angle θ , then the ray encounters a

reflective material with a radius of curvature r_1 , the new height h_1 , and new angle θ_1 , can be calculated using the following matrix equation.

$$\begin{pmatrix} \theta_1 \\ h_1 \end{pmatrix} = \begin{pmatrix} 1 & -\frac{2n_1}{r_1} \\ 0 & 1 \end{pmatrix} \cdot \begin{pmatrix} \theta \\ h \end{pmatrix} \quad (3)$$

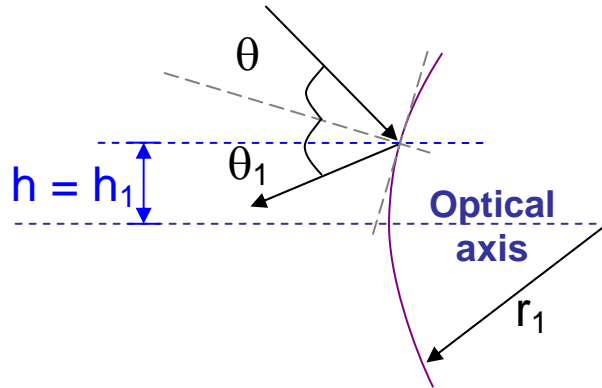


Fig. 3. Geometry of a ray experiencing reflection.

B. Component Modeling using Geometrical Matrices

Using these three geometrical matrix building blocks, one can develop models for optical system components. The geometrical matrices are simply multiplied together to create system matrices for the components. Each component's system matrix is used in the simulation by multiplying it by a subset of the current state matrix, to determine the new parameters for the new state matrix. The general equation used to calculate the new variables is

$$\begin{pmatrix} \text{New} \\ \text{State_Vector} \end{pmatrix} = \begin{pmatrix} \text{System} \\ \text{Matrix} \end{pmatrix} \cdot \begin{pmatrix} \text{Current} \\ \text{State_Vector} \end{pmatrix}. \quad (4)$$

Notice that in both figures 2 and 3 there is a discrepancy in the distance that the ray traverses to the surface of the optical element. Although this error is exaggerated in the figures, this error is assumed to be negligible by the paraxial ray assumptions [1].

1) *Lenses*: Because the thickness of a MOEMS lens is comparable to the radius of curvature of the lens, it is necessary to use the thick lens formulations and not the thin lens approximations [2]. See Fig. 4 for a diagram of the thick lens geometry.

In the case of the thick lens the first matrix required for the component model is the refraction matrix for the incident surface of the lens. The second matrix is a translation matrix for the distance traversed within the lens. The third matrix describes the refraction effects as the optical path exits the second surface of the lens. Multiplying the matrices together yields the system matrix for a thick lens component (5).

$$\begin{pmatrix} 1 & \frac{(n_2-n_1)}{r_2} \\ 0 & 1 \end{pmatrix} \cdot \begin{pmatrix} 1 & 0 \\ \frac{t_2}{n_2} & 1 \end{pmatrix} \cdot \begin{pmatrix} 1 & \frac{(n_1-n_2)}{r_1} \\ 0 & 1 \end{pmatrix} = \begin{pmatrix} \frac{r_2 \cdot n_2 + t_2 \cdot n_1 - t_2 \cdot n_2}{r_2 \cdot n_2} & (n_2 - n_1) \cdot \frac{-r_2 \cdot n_2 + t_2 \cdot n_1 - t_2 \cdot n_2 + n_2 \cdot r_1}{r_1 \cdot r_2 \cdot n_2} \\ \frac{t_2}{n_2} & \frac{r_1 \cdot n_2 - t_2 \cdot n_2 + t_2 \cdot n_1}{r_1 \cdot n_2} \end{pmatrix} \quad (5)$$

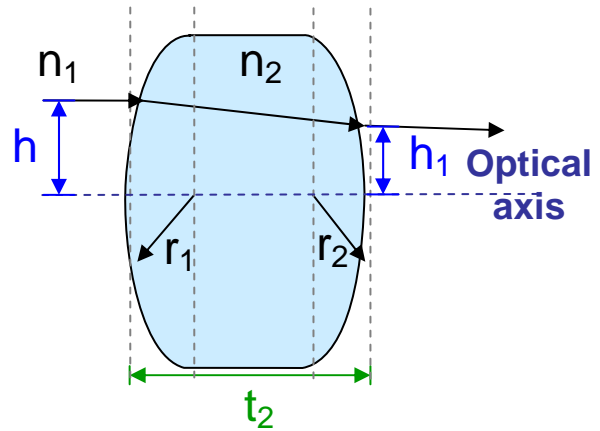


Fig. 4. Thick lens Geometry

A thin lens formulation can only be accurately used if the radius of curvature is much larger than the thickness of lens. See Fig. 5 for a diagram of the thin lens geometry. In the thin lens case, the component system matrix is reduced to simply the refraction matrix for the incident surface of the lens and the refraction matrix for the second surface of the lens as in (6).

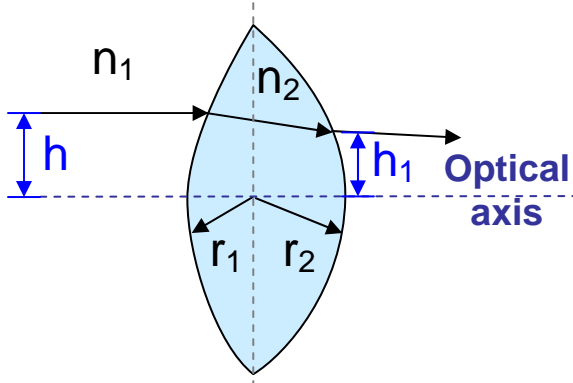


Fig. 5. Thin lens Geometry

$$\begin{pmatrix} 1 & (n_2 - n_1) \\ 0 & 1 \end{pmatrix} \begin{pmatrix} 1 & (n_1 - n_2) \\ 0 & 1 \end{pmatrix} = \begin{pmatrix} 1 & n_2 - n_1 \cdot \left(\frac{1}{r_1} - \frac{1}{r_2} \right) \\ 0 & 1 \end{pmatrix} \quad (6)$$

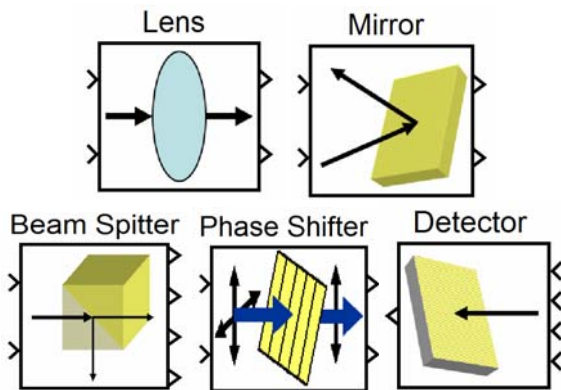


Fig. 6. Icons for the toolbox library (Lens, Mirror, Beam Splitter, Wave Plate, and Detector).

The icons shown in Fig. 6 are Simulink hierarchical constructs that include implementations of the system matrices. The icons of the toolbox library implement basic optical components such as a Lens, Mirror, Beam Splitter, Wave Plate, and a Photo-EMF Detector. The Lens icon is a Simulink subsystem that is masked. After placing the icon, you can double click upon it to bring up the subsystem shown in Fig. 7.

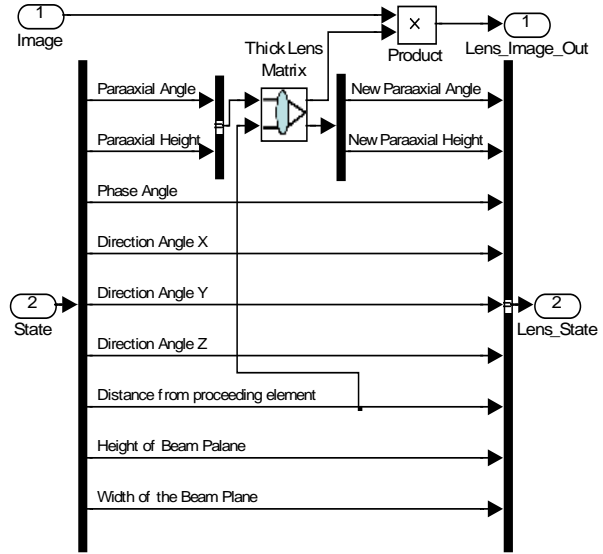


Fig. 7. Laser ultrasound thick lens system matrix.

This subsystem illustrates the connections between the state vector and the image that are passed to the lens system matrix. Only the paraxial angle, paraxial height and the distance from the preceding element are passed to the thick lens system matrix. The thick lens matrix is also masked, and when it is clicked will bring up a window for typing in parameters (Fig. 8). In this window the lens thickness, the two radii, and the two indices of refraction can be input.

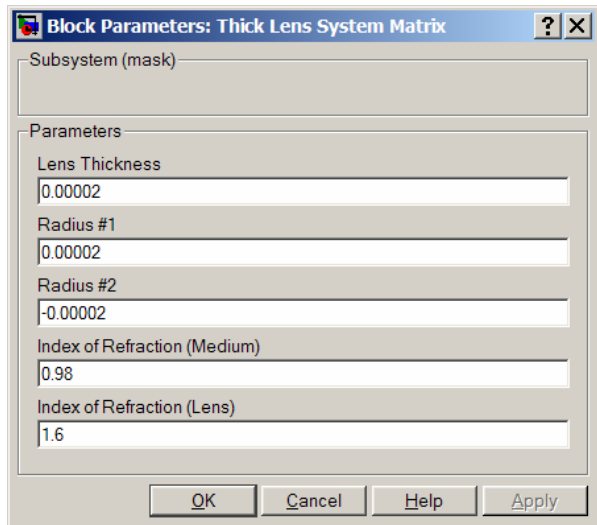


Fig. 8. Thick lens parameters window.

If you look under the mask for the thick lens system matrix you will see the block diagram in Fig. 9. In this block the distance from the preceding optical element (Input 2) is passed to the translation matrix. The translation matrix is multiplied by the refraction matrix for the first surface of the lens. The result is multiplied by the transfer matrix for translation that occurs between the lens surfaces. The resultant is multiplied by the refraction matrix for the second lens surface. The final result is the system matrix for the thick lens. This matrix is multiplied by the paraxial angle and height (Input 1) to give the new paraxial angle and height which are passed to the next optical element (Output 2). The magnification factor is also computed (Output 1). The magnification is simply the negative inverse of the element (2, 2), or using the ABCD matrix notation the magnification is $-1/D$.

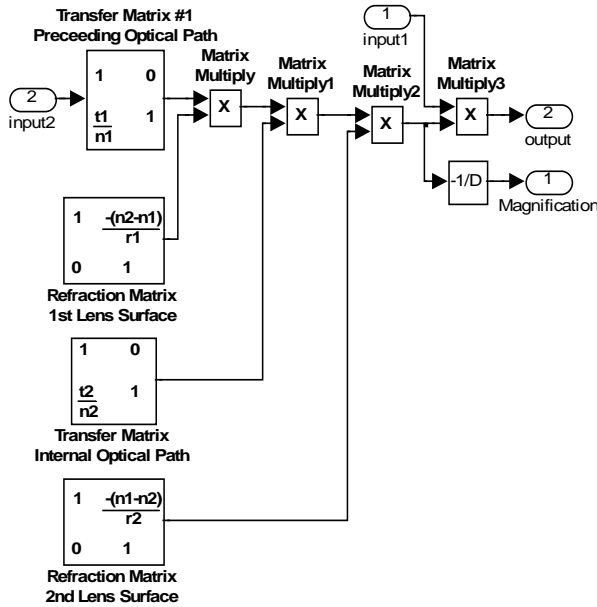


Fig. 9. Thick lens system matrix.

In the next level up (Fig. 7) we see that the lens magnification which was output by the thick lens system matrix is multiplied by the image matrix to adjust the intensity. All of the unchanged signals, along with the new paraxial angle and height are passed to the next optical element.

2) *Mirrors*: Fig. 10 shows the diagram of the mirror geometry. The system matrix for a mirror is that of a simple reflector (7) is

$$\begin{pmatrix} \text{Mirror} \\ \text{System} \\ \text{Matrix} \end{pmatrix} = \begin{pmatrix} 1 & -\frac{2n_1}{r_1} \\ 0 & 1 \end{pmatrix}. \quad (7)$$

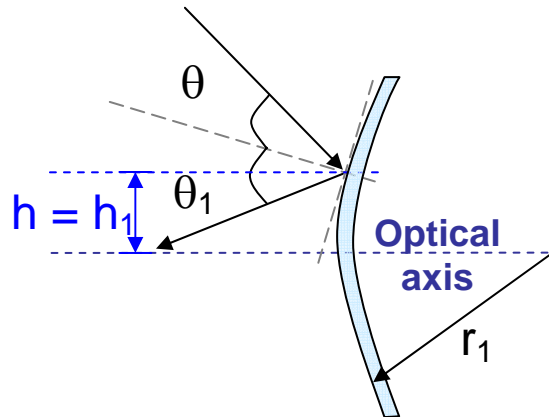


Fig. 10. Mirror Geometry

The mirror system matrix block is masked, so double clicking upon the mirror icon will bring up the block parameter window (Fig. 11). The block parameter window is where mirror parameters such as the mirror angle, etch hole size, etch hole spacing, the index of refraction for the mirror material and the radius of curvature for the mirror are entered.

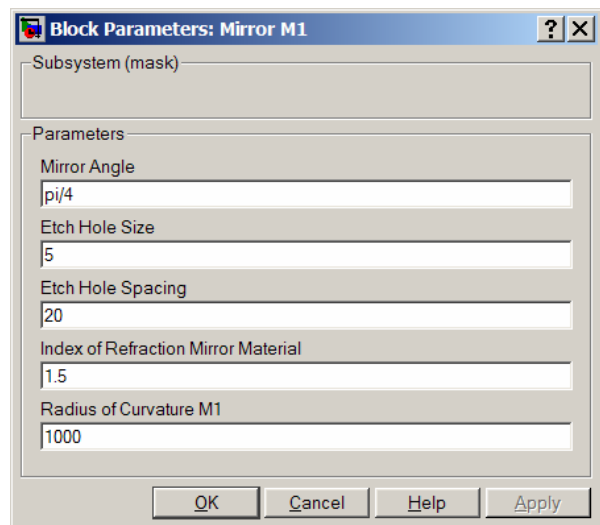


Fig. 11. Mirror parameters pop up window.

Underneath the subsystem mask is the mirror system matrix block (Fig. 12). The mirror system block uses the paraxial angle and height, along with the directional angle x . The mirror system matrix is multiplied by the paraxial angle and height to give the new paraxial angle and height. The direction angle x is modified according to the law of reflection. The direction angle is also used to calculate the angle of incidence at the surface of the mirror which is used for de-rating the intensity of light reflected from the mirror surface.

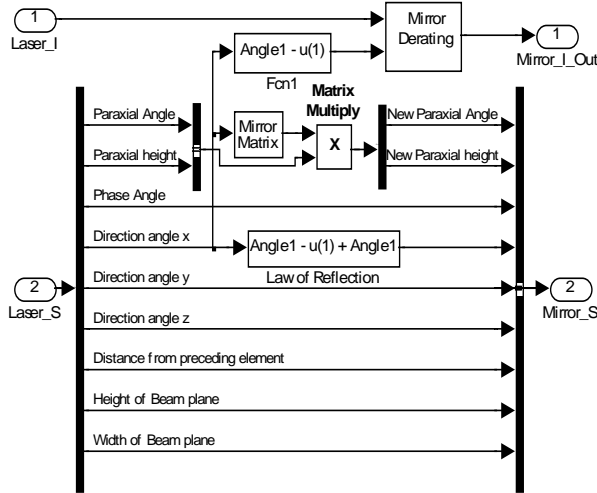


Fig. 12. Mirror system matrix

The mirror matrix block (Fig. 13) determines the systems matrix for the mirror. In this block the translation matrix for the light beam from the preceding optical element to the mirror is multiplied by the mirror reflection system matrix to give the overall system matrix for a mirror.

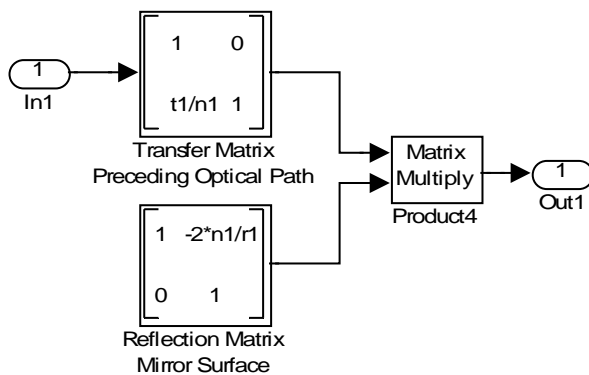
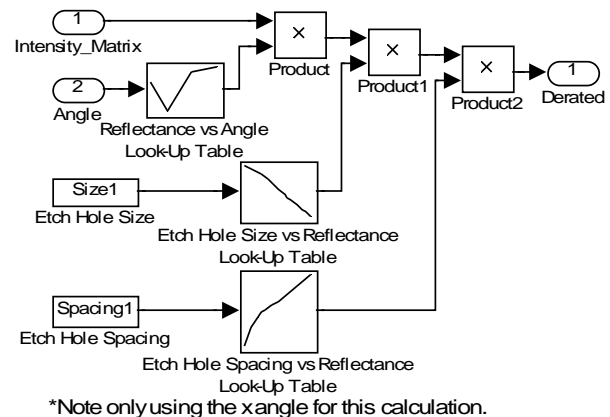


Fig. 13. Mirror system matrix.

Many MOEMS devices are required to have etch holes so that the release etchant can flow under the device and insure the complete removal of a sacrificial layer. This allows moving parts to be free from any substrate or unwanted attachments. Because etch holes have a large effect on the reflectivity of MOEMS mirrors they have been included in the models. Using data from [3], and lookup tables in Simulink®, a block has been developed that takes into account etch-hole size and spacing, as well as the angle of the mirror when determining the intensity of light that is reflected from a MOEMS mirror.

The angle of incidence at the surface of the mirror is passed to a mirror de-rating block (Fig. 14). In this block the intensity of the reflected light is reduced using three factors. First the reflectance is reduced according to the angle of incidence. For this block look up tables are used to determine the outputs. The result from the reflectance block is multiplied by a look up table block that determines the reduction in light intensity due to the size of the etch holes in the mirror surface. Since almost all of the pop up MOEMS elements require etch holes for the elements to be released from the substrate, this is a real world issue that needs to be addressed. The result from this block is multiplied by the result of a look up table for the reduction in light intensity due to the spacing of the etch holes. The overall result of this block is multiplied by the image to reduce the intensity of light of the image that is passed to the next optical element.



*Note only using the x angle for this calculation.

Fig. 14. Mirror de-rating block.

3) *Wave plates*: The wave plate used is a $\frac{1}{2} \lambda$ phase retarder and the source is linearly polarized. Fig. 15 shows a diagram of the wave plate geometry. Wave plates are used to rotate the phase angle of the outgoing light.

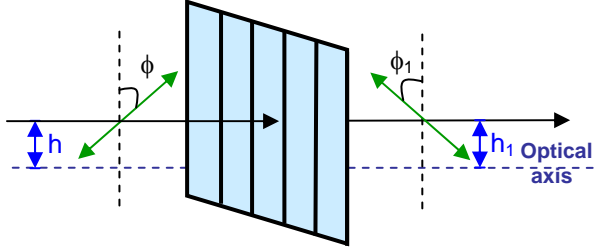


Fig. 15. Wave Plate Geometry

A rotation matrix like that of (8) could be used to determine the amount of phase rotation provided by a wave plate.

$$J_R = \begin{pmatrix} \cos(\theta) & \sin(\theta) \\ -\sin(\theta) & \cos(\theta) \end{pmatrix} \quad (8)$$

However for our application which uses a half wave plate and assumes that the source is linearly polarized, the equations simplify to the level where matrices are not required. For this application we first look at the electric field as it is split into its x and y components as is given in (9).

$$\begin{pmatrix} E_X \\ E_Y \end{pmatrix} = \begin{pmatrix} \frac{1}{\sqrt{2}} \cdot E_0 \\ \frac{1}{\sqrt{2}} \cdot E_0 \end{pmatrix} \quad (9)$$

Where E_0 is the initial total electric field and E_X and E_Y are the perpendicular and parallel components. These components can be used to calculate the angle of phase rotation for the half wave plate. By multiplying (9) by a matrix that represents linearly polarized light we get equations (10, 11) [4].

$$E'_X = \cos(\theta) \cdot E_X \quad (10)$$

$$E'_Y = -\sin(\theta) \cdot E_Y \quad (11)$$

Equations (10, 11) are used in (12) to determine the angle of phase rotation (α), given a mechanical rotation of the wave plate by angle θ .

$$\tan(\alpha) = \frac{E'_Y}{E'_X} = \frac{-\sin(\theta)}{\cos(\theta)} = \tan(-\theta) \quad (12)$$

So the angle of phase rotation simplifies to

$$\alpha = -\theta. \quad (13)$$

The intensity of the light (I) that has passed through the wave plate is found by

$$I = \sqrt{(E'_X)^2 + (E'_Y)^2} \quad (14)$$

$$I = \sqrt{\left(\frac{1}{\sqrt{2}} \cdot \cos(\theta) \cdot E_0\right)^2 + \left(\frac{1}{\sqrt{2}} \cdot -\sin(\theta) \cdot E_0\right)^2} = E_0. \quad (15)$$

The total intensity of light remains unchanged by a rotation of phase angle (15); therefore the image is passed through the phase shift block without any modification (Fig. 16). This block passes all of the signals through unchanged, except the phase angle. The phase angle is modified in the $\frac{1}{2}$ wave plate sub-block.

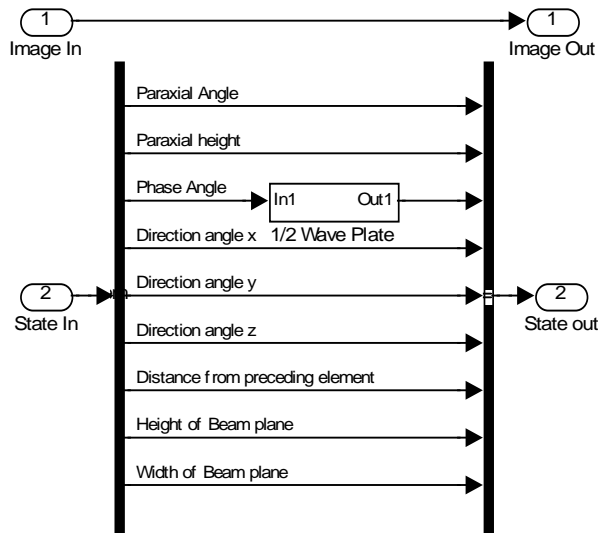


Fig. 16. Phase shifting wave plate block.

The half wave plate sub-block is masked, so it will open a block parameter window (Fig. 17). In this window there is only one parameter, the mechanical angle of rotation for the half wave plate. This parameter is used to adjust the relative intensities between the reference beam, and the transmission beam that has been directed at the surface of the material under test.

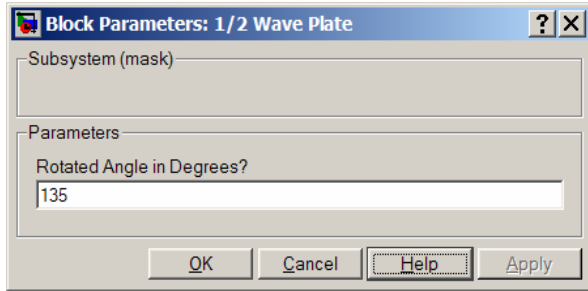


Fig. 17. $\frac{1}{2}$ Wave plate phase parameters pop up window.

If you look under the mask for the half wave plate you will see a single function block (Fig. 18). In this simple block the phase angle is multiplied by -1 to accomplish a $2*\theta$ rotation in phase angle in the opposite direction.

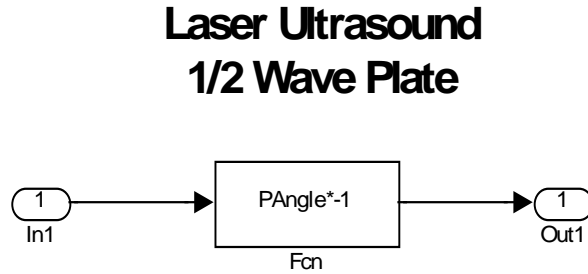


Fig. 18. $\frac{1}{2}$ Wave plate phase shifting block.

4) *Beam splitters:* A beam splitter is modeled as a plane mirror with variable reflectivity and transmission. See Fig. 19 for a diagram of the beam splitter geometry. The reflectance matrix mentioned earlier (3) is for a curved mirror surface and must be modified for a plane mirror. To formulate the matrix for a plane mirror, you must take the limit of the power of the surface as the radius goes to infinity, which will go to zero [5].

$$\lim_{r \rightarrow \infty} -\frac{n'_1 - n_1}{r} = 0 \quad (16)$$

The zero for that element in the matrix results in the plane mirror reflectance matrix reducing to the identity matrix:

$$\begin{pmatrix} 1 & 0 \\ 0 & 1 \end{pmatrix}. \quad (17)$$

The system matrix of the component can be formulated (18) for the beam splitter by starting with a translation matrix that accounts for the distance and medium from the source to the plane mirror surface. The second matrix is the reflection matrix for the surface of the beam splitter.

$$\begin{pmatrix} 1 & 0 \\ \frac{t_1}{n_1} & 1 \end{pmatrix} = \begin{pmatrix} 1 & 0 \\ \frac{t_1}{n_1} & 1 \end{pmatrix} \cdot \begin{pmatrix} 1 & 0 \\ 0 & 1 \end{pmatrix} \quad (18)$$

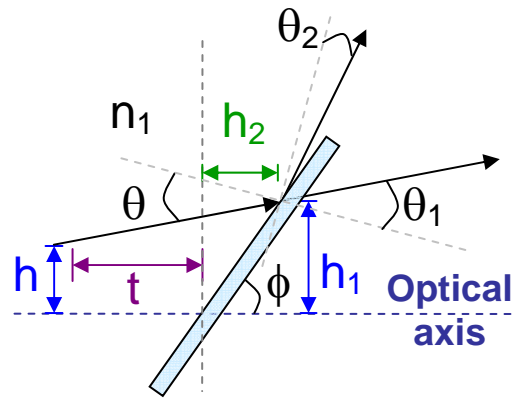


Fig. 19. Beam Splitter Geometry

The beam splitter sub-block (Fig. 20) has a single image and state vector as inputs but has two images and state vectors for outputs. In this block the phase angle is used to determine the two relative intensities of light that multiplied by the input image to create the two new images that are passed to the next optical elements. Also, the direction angle X is modified for one of the state vectors by adding a constant shift of 90° , while the other state vector direction angle X remains unchanged. This corresponds to the two light

paths that emerge from a beam splitting cube, where one light path passes directly through the cube, but the second path emerges from an orthogonal face of the cube.

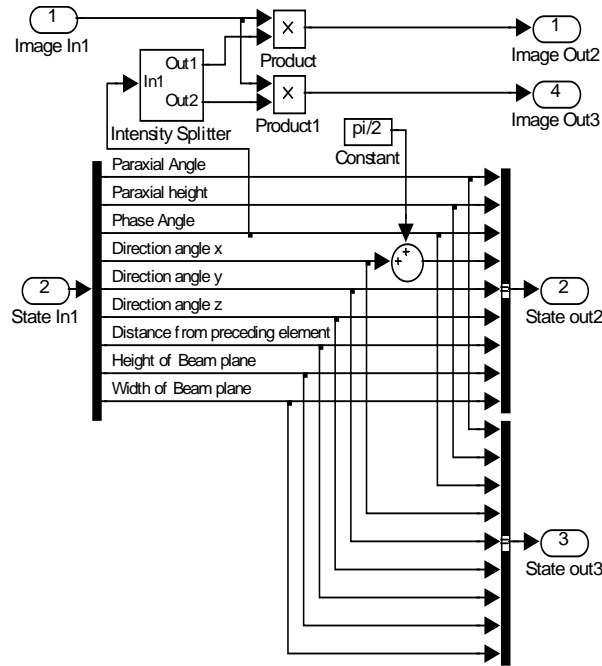


Fig. 20. Beam Splitter Block.

The intensity splitter (Fig. 21) uses the phase angle to generate four different linear sections. The phase angle is also used to control the switches which select one of four linear functions to be output. The first function starts at zero and goes to one for a phase angle of 90° . The second function starts at one and goes to zero for a phase angle of 180° . The third function starts at zero and goes to one for a phase angle of 270° . The fourth function starts at one and goes to zero for a phase angle of 360° .

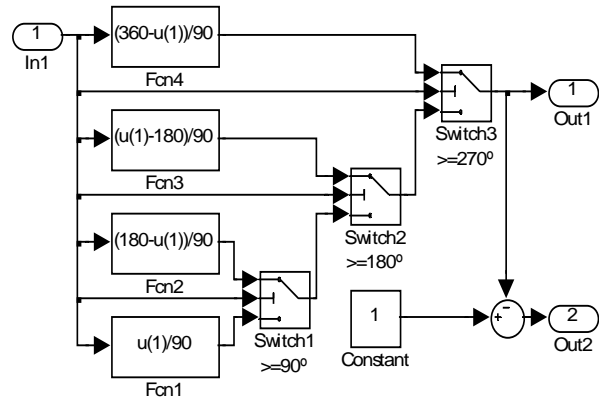


Fig. 21. Beam splitter intensity splitter block.

Switch 1 outputs function 1 when the phase angle is less than 90° , and outputs function 2 when the phase angle is equal or greater than 90° , and less than 180° . When the phase angle is less than 270° and is greater than or equal to 180° switch 2 outputs function 3. If the phase angle is less than 180° then the output of switch 1 is passed through switch 2. When the phase angle is 360° or less and is greater than or equal to 270° switch 3 outputs function 4. If the phase angle is less than 270° then the output of switch 2 is passed through switch 3. In this manner all four functions can be output in the proper sequence, thus insuring that the output intensity will properly vary as the phase rotates through 360° .

5) *Photo-EMF Detector*: Modeling of the laser ultrasonic receiver necessitated the modeling of the detector. For our application we modeled a Photo-EMF detector at the most rudimentary level. The detector block (Fig. 22) provides a sink for all of the state vector information in the form of a scope. The block receives two images as inputs. These are the reference beam image and the reflected measurement beam image. The reference beam image is subtracted from the reflected measurement beam image to give a time varying signal. This signal, which is roughly equivalent to a single pixel difference of the input images, is passed to the highest level of the Simulink model as the ultimate output from the system (Bottom graph of Fig. 23).

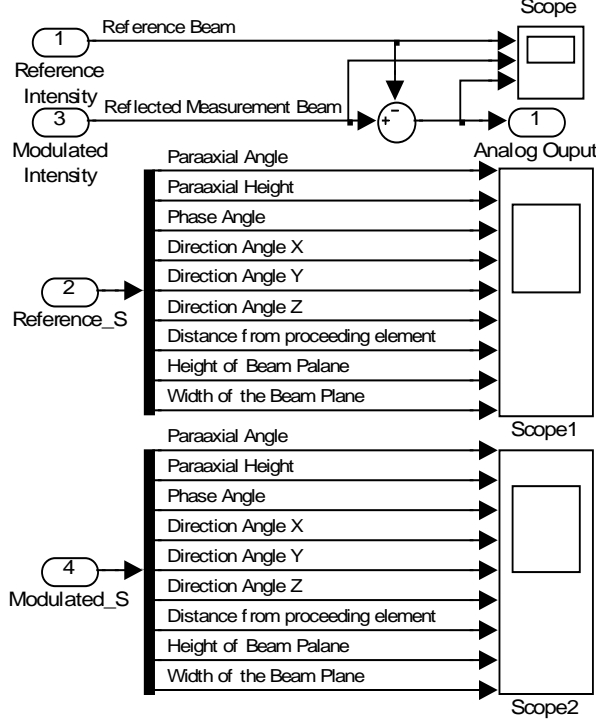


Fig. 22. Photo-EMF detector block.

Gaussian Constants

The Gaussian constants can be used to determine a variety of properties relating to the component. They can be taken directly from the final system matrix for each component. The constants are found in the order shown below:

$$\begin{pmatrix} b & -a \\ -c & d \end{pmatrix}. \quad (19)$$

The principal focus point can be determined by:

$$f = \frac{1}{a}. \quad (20)$$

The magnification factor is given by:

$$\mu = \frac{1}{b \cdot s_0} \quad (21)$$

where

$$s_0 = -t. \quad (22)$$

The image position is found to be:

$$S = \frac{d + c \cdot s_0}{b + a \cdot s_0}. \quad (23)$$

The principal foci are determined by:

$$S_u = \frac{c - 1}{a} \quad (24)$$

$$S_{u0} = \frac{1 - b}{a}. \quad (25)$$

The nodal points are given by:

$$S_N = \frac{c - \frac{n_1}{a}}{\frac{n_2}{a}} \quad (26)$$

$$S_{N0} = \frac{\frac{n_1}{a} - b}{\frac{n_2}{a}}. \quad (27)$$

These parameters can be used to modify the image (plane wave) that is being modeled in an application. For information on matrix optics or Gaussian constants refer to [1, 6].

C. Other Modeling Techniques

In addition to matrix optical modeling, electrical, mechanical and other optical models can be created. New optical components such as micro lenses can be added to the library. Micro lenses from $5\mu\text{m}$ to $750\mu\text{m}$ have been fabricated using photoresist [7]. These lenses are roughly hemispherical in shape, and the surface deviation is on the order of one tenth of a wave [8]. For this application, the diameter of the photoresist lens can be used in our lens model as one of the lens radii. The index of refraction for the common photoresist lens material PMMA is 1.5014 [9]. Diffractive optical models can also be added to the library. In the future, mechanical and

electrical parameters will be added to the component models. Models can be created for mechanical components such as cantilever beams and bridges with both point and distributed loads. Electrical components that could be modeled include electrostatic gap closer actuator and various detectors for the system. Although we have not developed these components yet, they could easily be incorporated into the system framework that we have developed.

IV. System Model of A MOEMS Laser Ultrasonic Receiver System

A MOEMS-based laser ultrasonic receiver system has been chosen as the example to be used to investigate system modeling using the MOEMS toolbox. The MOEMS-based laser ultrasonic receiver system can be realized using micro optical components that are assembled on a silicon wafer (Fig. 24). Refer to [10, 11] for the basics of laser ultrasonics. This system is of interest for advanced nondestructive evaluation (NDE) technologies (for assuring the integrity of airframe structures, wiring, etc.) at NASA Langley Research Center [12, 13]. Laser ultrasonic inspection instruments have been shown to detect delaminations and fatigue cracks in critical structures [14]. However, laser based inspection instruments are generally too bulky to be used in the confined spaces that are typical of space and aircraft inspection sites. MOEMS is a key technology to reducing the size of current instruments and enabling increased inspection coverage in areas that were previously inaccessible due to instrument size and weight.

This type of laser ultrasonic receiver is comprised of a laser and an optical system that detects the ultrasonic waves. The laser beam is reflected off a material in which ultrasonic waves have been created. The laser beam interacts with induced ultrasonic waves creating a reflected beam that is ultrasonically modulated. This reflected beam is directed by the micro-optical components to a photo-emf detector where the beam is combined with a reference beam to demodulate the ultrasonic signal [15]. The

system is an interferometer which has a photo-emf detector that outputs a signal that is proportional to the velocity of the fringe line movement. Material integrity is established by analysis of the demodulated signal.

The laser ultrasonic receiver system is modeled in the time domain using plane waves that are represented by images that are passed to each component. The state vector passes parameters to each component that are used to calculate any images transformations. This is how information is passed between the components of the receiver system.

The entire laser ultrasonic receiver system is modeled hierarchically using Simulink[®]. The optical subsystem (Fig. 25) is one of many blocks and uses the MOEMS toolbox components to model the optical performance of the MOEMS devices. The optical system is divided into three paths; a transmission beam path on top, a reference beam path, and a modulated beam path shown on the bottom of Fig. 25. The transmission path has two inputs found on the upper left side of the diagram, the state vector, and an image of the initial laser beam plane wave. The laser beam is passed through a mirror and a phase shifting wave plate before entering the beam splitter. The reflected beam from the beam splitter becomes the transmission beam. The transmission beam path passes through a lens to another wave plate, to a second lens, and finally through a mirror and out as both an image and as a state vector. Both of which are sent to the material under test.

The reference beam is the beam splitter's transmitted beam. The reference beam is passed to a mirror where it is redirected to the detector. This beam is necessary for demodulating the analog signal.

The lower set of inputs on the right side of the diagram represents the modulated beam path. This path begins with the transmission beam after it has reflected off of the material under test. In this design the beam must retrace through the optical path to reach the detector. At the detector

both the reference beam and the modulated beam are summed destructively to generate an analog signal. By analyzing the time of flight between the two pulses a determination can be made about the integrity of the material under test.

Fig. 23 is a plot of the reference beam (top trace), the reflected measurement beam called the modulated beam (middle trace), and the analog signal generated by the detector (bottom trace). The sinusoidal waves represent the wave front phase of the plane wave images as they pass through a single point on the image plane. The red circles on the Modulated Beam graph highlight the areas where the ultrasonic signal is visibly modulated onto the carrier wave. The detector trace clearly shows the initial ultrasound pulse created within the material. It also shows the second pulse that is reflected from the back side of the material or a discontinuity within the material. By analyzing the time of flight between the two pulses a determination can be made about the integrity of the material under test.

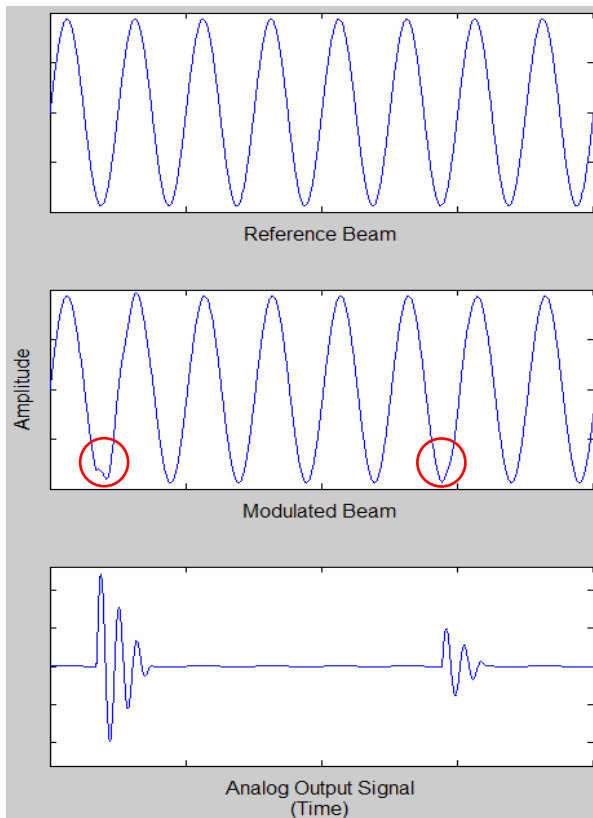


Fig. 23. Plot of the laser ultrasonic receiver signals

V. Conclusion

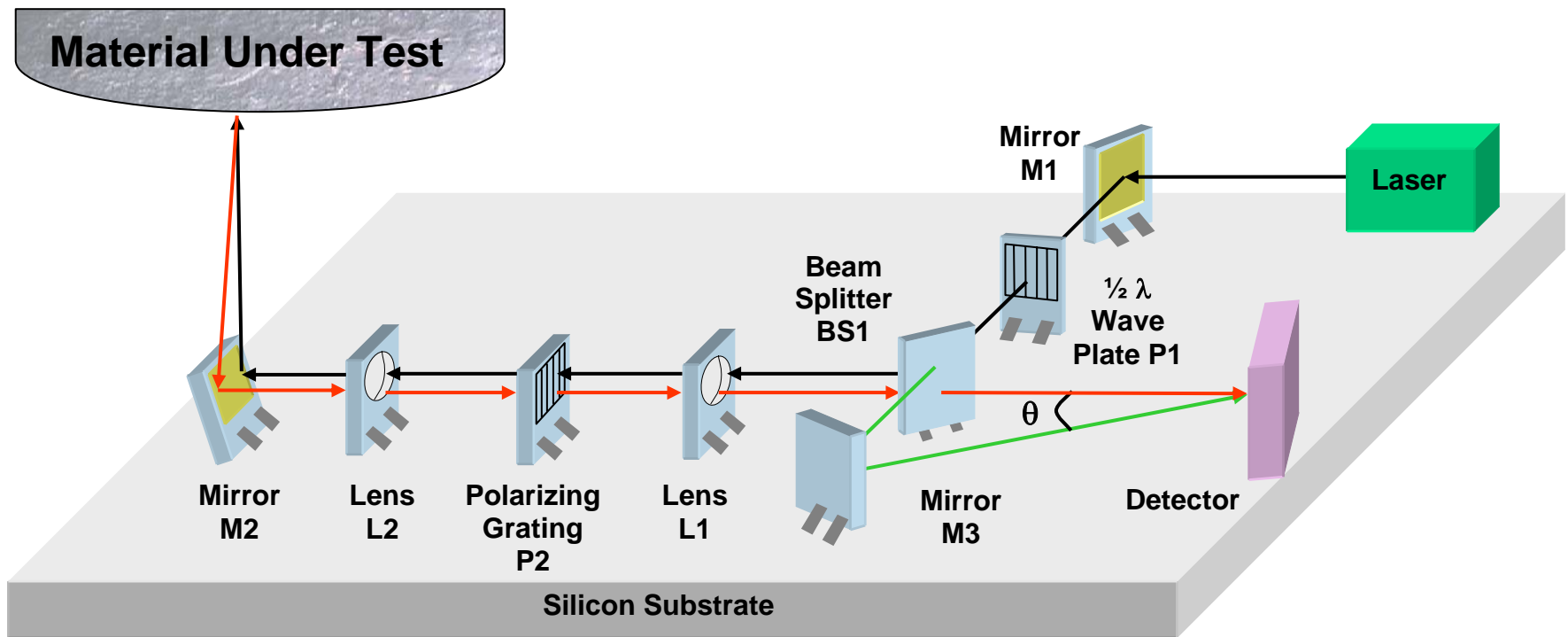
A geometrical matrix optical toolbox for use with Mathwork's Simulink[®] program has been developed. The MOEMS toolbox contains the basic elements for optical system modeling; thick and thin lenses, a mirror, a beam splitter, a wave plate and a translation block. In addition to the optical components, it includes a block that models the effects of etch holes in MEMS mirrors.

Modeling toolboxes allow users to spend more time investigating systems and design issues and less time developing component models. This toolbox was developed to facilitate rapid modeling of MOEMS systems; specifically a laser based ultrasonic receiver system being developed by NASA LaRC. The MOEMS toolbox can also be used for rapid prototyping of optical systems.

In the future we plan on adding more components to the toolbox. We also intend to fabricate the laser ultrasonic receiver system to verify the simulation results generated by our system model.

VI. References

- [1] Gerrard, A., Burch, J. M., "Introduction to Matrix Methods in Optics", John Wiley & Sons, London, 1975, pp. 32-33.
- [2] Allen Nussbaum, Richard A. Phillips, "Contemporary Optics for Sci. & Eng.", Prentice Hall Inc., Englewood Cliffs, 1976, pp. 5-35.
- [3] D. Goldstein, *Polarized Light*, 2d Ed., Chap. 11, (Marcel Dekker, Inc., New York, 2003, pp. 211-240.
- [4] Warren J. Blaker, "Geometric Optics: The Matrix Theory", Marcell Dekker Inc. New York, 1971 pp. 22-24.
- [5] J. Alda, "Paraxial Optics", Encyclopedia of Optical Engineering", Driggers, R., Ed., Marcel Dekker Inc., New York, 2003, pp. 1920-1931.
- [6] Jun Zou; M. Balberg, C. Byrne, Liu Chang; D.J. Brady, Optical properties of surface micromachined mirrors with etch holes, MEMS, Journal of , Vol. 8, Issue. 4 , Dec. 1999, pp. 506 - 513
- [7] D. Daly, R. Stevens, M. Hutley, N. Davies, "The Manufacture of Microlenses by Melting Photoresist", MicroLens Arrays, IOP Pub. Ltd., Bristol, pp. 23-34.
- [8] T. R. Jay, M. B. Stern, and R. E. Knowlden, "Effect of refractive microlens array fabrication parameters on optical quality," SPIE Proc. Vol. 1751, Miniature & Micro-Optics: Fabrication and System Applications II, July 19-20 1992, San Diego, pp. 236-245
- [9] Gregory T. A. Kovacs, "Micromachined Transducers Sourcebook", New York: McGraw-Hill, 1998, pp. 490.
- [10] Jean-Pierre Monchalin, Christian Néron, Jean F. Bussière "Laser-ultrasonics: from the laboratory to the shop floor", Physics in Canada, March, Vol. 51 No 2, <http://www.ultraoptec.com/press/j-p-ph.html>.
- [11] M. Klein, B. Pouet, P. Mitchell, "Photo-emf detector enables laser ultrasonic receiver", Detectors, Laser Focus World, Aug. 2000, url: <http://www.newport.com/Support/MagazineFeatures/00390-687.pdf>
- [12] Charles E. Harris, James H. Starnes, Jr., and Mark J. Shuart, "An Assessment of the State-of-the-Art in the Design and Manufacturing of Large Composite Structures for Aerospace Vehicles", NASA Technical Memorandum NASA/TM-2001-210844, Langley Research Center, Hampton, Virginia, April 2001, pages 50.
- [13] W. H. Prosser, T. L. Brown, S. E. Woodard, G. A. Fleming, and E. G. Cooper, "Sensor Technology for Integrated Vehicle Health Management of Aerospace Vehicles", AIP Conference Proceedings, March 27, 2003, Volume 657, Issue 1, pp. 1582-1589.
- [14] C. B. Scruby, L. E. Drain, "Laser Ultrasonics: Techniques and Applications", Adam Hilgar, Bristol, 1990, pp. 325-353.
- [15] David M. Pepper, "The Emergence of Nonlinear Optics in the Factory", Optics and Photonics News Magazine, May 1997.



- Transmission Beam Path
- Modulated Beam Path
- Reference Beam Path

Fig.24. A MOEMS Laser Ultrasonic Receiver System

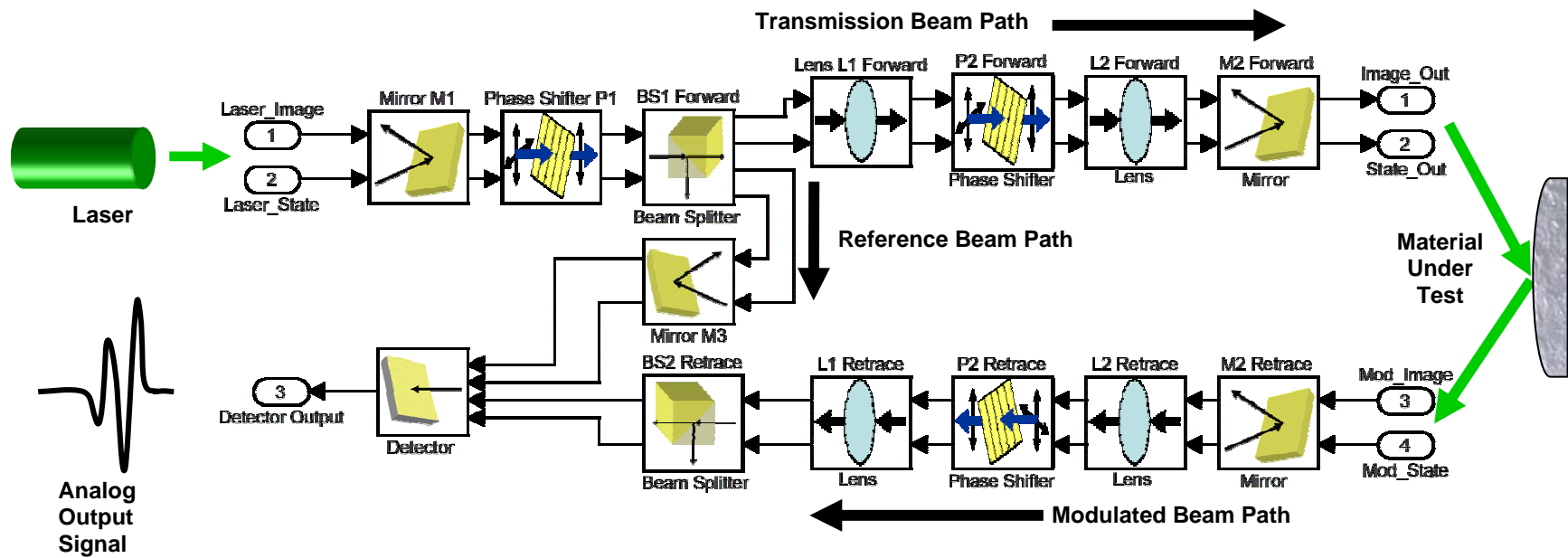


Fig.25. Block Diagram of Optical Subsystem

REPORT DOCUMENTATION PAGE				Form Approved OMB No. 0704-0188	
<p>The public reporting burden for this collection of information is estimated to average 1 hour per response, including the time for reviewing instructions, searching existing data sources, gathering and maintaining the data needed, and completing and reviewing the collection of information. Send comments regarding this burden estimate or any other aspect of this collection of information, including suggestions for reducing this burden, to Department of Defense, Washington Headquarters Services, Directorate for Information Operations and Reports (0704-0188), 1215 Jefferson Davis Highway, Suite 1204, Arlington, VA 22202-4302. Respondents should be aware that notwithstanding any other provision of law, no person shall be subject to any penalty for failing to comply with a collection of information if it does not display a currently valid OMB control number. PLEASE DO NOT RETURN YOUR FORM TO THE ABOVE ADDRESS.</p>					
1. REPORT DATE (DD-MM-YYYY)		2. REPORT TYPE		3. DATES COVERED (From - To)	
01- 10 - 2005		Technical Publication			
4. TITLE AND SUBTITLE MOEMS Modeling Using the Geometrical Matrix Toolbox				5a. CONTRACT NUMBER	
				5b. GRANT NUMBER	
				5c. PROGRAM ELEMENT NUMBER	
6. AUTHOR(S) Wilson, William C.; and Atkinson, Gary M.				5d. PROJECT NUMBER	
				5e. TASK NUMBER	
				5f. WORK UNIT NUMBER 23-064-30-12	
7. PERFORMING ORGANIZATION NAME(S) AND ADDRESS(ES) NASA Langley Research Center Hampton, VA 23681-2199				8. PERFORMING ORGANIZATION REPORT NUMBER L-19179	
9. SPONSORING/MONITORING AGENCY NAME(S) AND ADDRESS(ES) National Aeronautics and Space Administration Washington, DC 20546-0001				10. SPONSOR/MONITOR'S ACRONYM(S) NASA	
				11. SPONSOR/MONITOR'S REPORT NUMBER(S) NASA/TP-2005-213931	
12. DISTRIBUTION/AVAILABILITY STATEMENT Unclassified - Unlimited Subject Category 33 Availability: NASA CASI (301) 621-0390					
13. SUPPLEMENTARY NOTES An electronic version can be found at http://ntrs.nasa.gov					
14. ABSTRACT New technologies such as MicroOptoElectroMechanical Systems (MOEMS) require new modeling tools. These tools must simultaneously model the optical, electrical, and mechanical domains and the interactions between these domains. To facilitate rapid prototyping of these new technologies an optical toolbox has been developed for modeling MOEMS devices. The toolbox models are constructed using MATLAB's dynamical simulator, Simulink. Modeling toolboxes will allow users to focus their efforts on system design and analysis as opposed to developing component models. This toolbox was developed to facilitate rapid modeling and design of a MOEMS based laser ultrasonic receiver system.					
15. SUBJECT TERMS EMS; Geometrical Optics; MOEMS; Optical Modeling; Ultrasonic Transducer					
16. SECURITY CLASSIFICATION OF:			17. LIMITATION OF ABSTRACT	18. NUMBER OF PAGES	19a. NAME OF RESPONSIBLE PERSON
a. REPORT	b. ABSTRACT	c. THIS PAGE			STI Help Desk (email: help@sti.nasa.gov)
U	U	U	UU	20	19b. TELEPHONE NUMBER (Include area code) (301) 621-0390